EUROPEAN ORGANIZATION FOR NUCLEAR RESEARCH

CERN-PPE/92-78
20.03.1992

The electrostatic field in microstrip chambers and its influence on detector performance.

J.J. Florent, J. Gaudaen, L. Ropelewski, F. Sauli

CERN, Geneva, Switzerland

Abstract

This paper describes the results of detailed field calculations for microstrip gas chambers. A program was written using the multigrid technique, which allows to do very fast electrical field calculations for two-dimensional geometries. Typical execution times for a problem on a grid with 154000 nodes are 125 s on a SUN IPC and 14 s on the CERN IBM 3090. The speed of this program makes it practical to do field calculations for a variety of geometries, materials and operating conditions. This has allowed us to gain a better understanding of important phenomena for the operation of gas microstrip chambers, such as charging of the dielectric support.

1. Introduction

The gas microstrip chamber has generated great interest recently as an alternative detector to solve the severe problem of tracking at the next generation of high luminosity hadron colliders [1 – 8]. The detector consists of a sequence of alternating thin conductive anode and cathode strips placed on an insulating support. The sensitive gas volume is closed by a drift electrode, and a field shaping electrode is usually provided on the backplane of the insulating support. Proportional amplification with gains above 10^4, very good energy resolution and localization accuracy, as well as high rate capability have been demonstrated.

From the quoted works it also appears clearly that the applied potentials and the nature of the insulating support are of crucial importance for correct operation of the detector. When using good insulators, charging up of the surface due to deposition of ions modifies dynamically the electric field and hence the operating characteristics. On the other hand, use of a low resistivity support introduces leakage currents and may lead to breakdown. A systematic study of the effects of charging can be found in [7],[?]. The present paper is an attempt to answer a number of questions concerning the effects of charging by doing extensive field calculations, including the effect of resistivity of the support. We will also try to deduce an optimal geometric configuration of the detector.

2. Field equations

2.1 Perfect insulators

In the simple case of perfectly insulating dielectric materials, the electrostatic potential ϕ_e obeys the equation

$$\nabla\cdot(\varepsilon\nabla\phi_e) = -\rho \tag{1}$$

where ε is the dielectric constant, and ρ is the free electric space charge density. The electric field strength is given by

$$\vec{E} = -\nabla\phi_e \tag{2}$$

In the absence of free charges and currents, and in a uniform medium, equation (1) reduces to the well known Laplace equation

$$\nabla^2\phi_e = 0 \tag{3}$$

The boundary conditions at the interface between two regions with dielectric constant ε_2 and ε_1 respectively, can be expressed as

$$(\varepsilon_2\vec{E}_2 - \varepsilon_1\vec{E}_1)\cdot\vec{n} = \sigma \tag{4}$$

$$(\varepsilon_2\vec{E}_2 - \varepsilon_1\vec{E}_1)\times\vec{n} = 0 \tag{5}$$

where σ represents the free surface charge and $\vec{n}$ is the unit vector perpendicular to the boundary, pointing from region 1 to region 2. When no free charges are present, (4) reduces to

$$\varepsilon_2 E_2^{\perp} - \varepsilon_1 E_1^{\perp} = 0 \tag{6}$$

where $E^{\perp}$ denotes the component of the field perpendicular to the boundary.

2.2 Conductive materials

When the substrate material is conducting, the situation becomes more complicated: for a linear isotropic medium with electric conductivity γ, Ohm's law states that a current will flow whose density is given by

$$\vec{J} = \gamma \vec{E} \tag{7}$$

Therefore, when field lines cross the boundary between substrate and gas, charge will accumulate on this boundary.This charge has to be taken into account when solving equations (1).

We could try to solve the problem iteratively, by applying Ohm's law to calculate the surface charge accumulated during a small time interval and entering this charge into the field equations (1) before starting the next iteration. However, this would take too long to be considered as a practical method. Fortunately, we can find the steady state field in the presence of conducting materials by solving a modified field equation given by

$$\nabla \cdot (\gamma \nabla \phi_e) = -j \tag{8}$$

where j is the electric current source density. As in the electrostatic field problem, the electric field is given by (2), and in a uniform medium without free charges or currents (8) can be reduced to the Laplace equation (3).

The difference between the two field configurations only shows up as a boundary condition between the substrate and the gas volume. From the similarity of the equations (1) and (8), it is easy to see that the boundary conditions for the current flow problem are given by

$$(\gamma_2 \vec{E}_2 - \gamma_1 \vec{E}_1) \cdot \vec{n} = j_s \tag{9}$$

and

$$(\gamma_2 \vec{E}_2 - \gamma_1 \vec{E}_1) \times \vec{n} = 0 \tag{10}$$

where j_s is a surface current source and $\vec{n}$ is the unit vector perpendicular to the surface, pointing from region 1 to region 2. For a conducting surface, with surface conductivity γ_s, the surface current source j_s becomes

$$j_s = \gamma_s \frac{\partial E^x}{\partial x} \tag{11}$$

Under normal circumstances, we can assume that the conductivity of the gas, $\gamma_2 = 0$, as well as the surface conductivity γ_s. The boundary condition for a conducting support then becomes

$$\gamma_s E^{\perp}_s = 0 \tag{12}$$

In other words, when the support is conducting, the equilibrium condition reached after charging up of the surface, is obtained when the field lines on the boundary between gas and support are parallel to the support. Note that this condition is only valid on the support side of the boundary! On the gas side, the field may or may not be parallel to the surface. This condition is easy to understand: we essentially ask that no more field lines cross the boundary from inside the support, so that no more charge can be transported to the surface. Fig. 1 illustrates the difference between a conducting and insulating medium: Fig. 1.a shows the field for a perfect insulator, Fig. 1.b shows the field obtained for the same voltages, but assuming a conducting support. Both cases correspond to a bad choice of potentials, since a number of field lines leaving the anode end up on the support.

The charge accumulated on the surface can in that case be calculated from (4):

$$\sigma = \varepsilon_0 E^{\nu}_{G} \tag{13}$$

where ε_0 is the dielectric constant of the vacuum and E^{ν}_{G} is the field component perpendicular to the surface in the gas volume. For the field configuration in Fig. 1b, this charge is shown in Fig. 1c.

3. Programming details

The standard way to solve boundary value problems is to define a set of grid points on which the partial differential equations and boundary conditions are expressed as finite difference equations. One then uses iterative techniques to solve the set of n equations in n unknowns, where n is the number of grid points. For reasons of speed, we have chosen to implement a so-called multigrid method. A very good description of this method can be found in [9] and will not be repeated here. The basic idea is to work not with a single grid, but with a sequence of grids of increasing fineness that constantly interact with each other. One can view the coarser grids as correction grids, accelerating the convergence on the finest grid by efficiently liquidating smooth error components. One can indeed verify that the convergence of classical relaxation schemes slows down as soon as the fluctuations of the residuals on the scale of the grid have been smoothed out.

Care must be taken in defining the grid points: it can be shown (see e.g. Durand [10]) that singularities (e.g. 90° angles) must coincide with grid points for the solution to converge to the correct value. To avoid all such problems, a grid generator is included in the program that makes all boundaries of the problem geometry coincide with grid lines. It also attempts to keep grids as square as possible, since we found that this can considerably improve the convergence of the method.

The implementation is done as a set of two programs: MSFIELD, which does the actual field calculations, and MSPLOT which uses the results of MSFIELD to produce a number of plots. Since the chambers have 4 electrodes, the field for a given set of potentials can be obtained as a linear combination of the fields calculated for 3 independent sets of potentials. Therefore MSFIELD calculates the field for 3 simple cases and stores the resulting field maps on disk. MSPLOT then uses these field maps to calculate and plot relevant quantities for any given set of potentials. To extract meaningful data from the computations and to facilitate comparison with experiment, MSPLOT also allows us to calculate gas gain as well as the diffusion of electrons transverse to the electric field. The latter gives some indication of avalanche size and the speed of charging up of the support, although more work is clearly needed to understand this phenomenon. The gas gain is calculated by integrating a parameterization of the Townsend coefficient along the field lines. At present a parameterization of the Townsend coefficient for a mixture Ar(90%)-CH4(10%) as a function of electric field strength is hard-coded in the program. A future version will allow the user to enter his own table of values of the Townsend coefficient versus electric field strength.

4. Results

4.1 Proportion of ions captured by cathodes

One of the arguments explaining the high rate capability of microstrip chambers has been that space charge is removed effectively because part of the ions produced in the avalanche only have to drift a small distance toward the cathode. One can estimate the fraction of ions drifting back toward the drift electrode by applying Gauss's law to a volume bounded by the drift electrode, the outermost field lines connecting this electrode to the anode, and the part of the anode between these field lines. This is illustrated in Fig. 2, which shows the integration contour and the variables used in the following formulas. In the absence of free charges, Gauss's law takes the form:

$$\int_S \varepsilon \vec{E} \cdot \vec{n} da = 0 \tag{14}$$

Along the field lines, the left hand side of (14) vanishes, so we are left with

$$\int_0^{x_1} \varepsilon_0 E^y_{an} dx = \int_0^{x_{cell}} \varepsilon_0 E^y_{drift} dx \tag{15}$$

The only unknown in this formula is x_1, the point which maps the drift electrode onto the anode. This point can therefore be calculated very easily if one knows the field values on the anode and drift electrode. Integrating the spatial distribution of ions along the anode from $-x_1$ to x_1 then yields the fraction of ions moving toward the drift region. The simplest approximation is obtained by assuming that the distribution of ions is uniform over the full width of the anode. In that case, the ratio of $2x_1$ to the width of the anode gives the proportion of ions drifting back towards the drift electrode. Fig. 3 shows how this proportion changes with increasing voltage on the drift electrode for a given set of potentials on anode, cathode and back plane.

4.2 Optimal field geometry

A priori, those ions that do not drift toward the drift electrode can not only end up on the cathode, but also on the surface of the support. This can be avoided by choosing a field configuration in which no field lines cross the surface. This field configuration can be found by applying (14), this time to a volume including the cathode, as illustrated by the contour marked (2) in Fig. 2. Our formula now becomes:

$$\int_0^{x_2} \varepsilon_0 E^y_{an} dx + \int_{x_{cat}}^{x_{cell}} \varepsilon_0 E^y_{cat} dx = \int_0^{x_{cell}} \varepsilon_0 E^y_{drift} dx \tag{16}$$

By forcing the field line connecting the edge of the cathode to the anode to arrive on the edge of the anode, i.e. $x_2 = x_{an}$, we ensure that no field lines cross the substrate surface. Since all field values can be expressed as linear combinations of the 3 independent electrode potentials, (16) becomes a linear equation in 3 unknowns. We therefore need two other equations to fix the potentials. Typically, we have chosen (15), as a second equation with a fixed fraction of ions going towards the drift electrode. This still leaves us the freedom to choose e.g. the anode potential so as to obtain a given gain. Fig. 4 shows an example of an optimal field configuration. Fig. 5 shows the experimentally measured variation of gain with rate for this field configuration and for two other ones for a detector made on HOYA

SL glass ($\rho = 2^{15}\Omega cm$ $\varepsilon_r = 4.9$). As can be seen, the rate dependence is reduced for the optimal configuration.

4.3 Investigation of different geometries and substrates

We can also investigate the effects of substrate thickness, anode width, cathode width etc. As an example, Fig. 6a shows the computed variation of gain as a function of anode width, keeping the anode voltage constant, but adjusting backplane and drift voltages so as to obtain an optimal field configuration for each geometry. Fig. 6b shows the effect of cathode width under the same conditions. From these plots it can be seen that one can increase the gain by reducing the size of the anodes, as could be expected, but also by increasing the size of the cathodes. This latter option might be preferable, since it is easier from a technological point of view and results in more robust detectors. The major limitation in this case will be surface flashover since the field strength between anode and cathode grows as the anode to cathode distance becomes smaller, even taking into account the reduction in anode voltage needed to obtain identical gas gain. Fig. 6c shows the dependence of gain on support thickness, with backplane voltage adjusted to keep the field configuration optimal. This plot clearly shows that one can almost completely cancel changes due to support thickness by adjusting the backplane voltage.

The program also allows us to study the effect of adding a thin layer of conductive material on the surface, either by ion implantation or some other means. Fig. 7 shows the effect of introducing a 4 micron thick layer with resistivity 10^{11} Ω.cm on top of a substrate with resistivity 10^{14} Ω.cm. This figure should be compared with Fig. 4, showing the field configuration for a chamber with identical geometry and voltages, but with a uniform substrate. As can be seen, the change is quite drastic. The main effect is a reduction of peak field associated with the edges of anode and cathode strips. Fig. 8 shows the component of the electric field parallel to the surface between anode and cathode, with and without the conductive layer. In this figure, the anode voltage for the configuration with a conductive layer was increased by 150V (to 800V) in order to obtain an identical gas gain for both cases. As can be seen, in the case of surface conductivity, the field strength is nearly constant, but about about twice as high as the minimum field strength obtained without surface conductivity. On the other hand, the peak field values associated with the edges of the electrodes are about 3 times higher in the absence of surface conductivity.

Two conflicting requirements guide the choice of substrate resistivity: in order to evacuate the charges deposited on the surface by avalanche formation we would like to have a small resistivity. On the other hand, a small resistivity means large currents flowing between electrodes, inducing noise and dissipating heat. For typical operating conditions, we find that the total anode current is about 200 to 300 pA/m for a material with bulk resistivity of 10^{14} Ωcm. To limit current noise below 1000 electrons rms for an amplifier shaping time of 10 ns, the maximum current per anode has to be less than 16 μA. For a detector with 10 cm long anodes this gives a lower limit on bulk resistivity of 10^8 Ωcm. A similar requirement on surface current leads to a minimum value for surface resistivity of about 3.10^{10} Ω/sq.

As discussed above, in conducting materials charge accumulates on the surface of the substrate until no more field lines cross the boundary. This modifies the field and therefore the gain of the chamber varies as a function of time, even without subjecting the chamber to ionizing radiation. The simplest estimate of this time constant is obtained by multiplying the bulk resistivity of the material with its dielectric constant $\tau = \rho \varepsilon_r \varepsilon_0$. For tedlar [7] ($\rho = 10^{14}\Omega$cm, $\varepsilon_r = 11$) this gives about 100 seconds. A somewhat more elaborate estimate can be made by calculating the accumulated charge on the surface for the equilibrium condition expressed by (12), and dividing it by the initial current flowing from the electrodes to the support surface. For our tedlar chambers, we have calculated these quantities for

a non-optimal operating condition as 1160 pC/m and 7 pA/m respectively. This gives a time constant of 165 seconds, in good agreement with the first estimate. The calculation actually predicts a slight increase in gain, which was indeed observed experimentally [7] , with about the same time constant.

From the point of view of detector performance, another important quantity are the capacitances between electrodes. These are show in Fig. 9.a to c for a detector that has an anode to anode pitch of 380 μm. Fig. 9a shows the dependence of capacitance on anode width, for a constant cathode width of 160 μm and a support thickness of 96 μm. Fig. 9b shows the dependence on cathode width, for the same support thickness and an anode width of 32 μm. Finally, Fig. 9c shows the effect of support thickness for a detector with 32 μm anodes and 160 μm cathodes. In all figures, the substrate material was tedlar, which has a relatively high dielectric constant of 11. For chambers on glass, the capacitances should be approximately divided by two. Total anode and cathode capacitances do not depend very strongly on support thickness or even cathode width. For the range of geometries explored, the total anode capacitance varies between 40 and 70 pF/m. In contrast the relative coupling between anode and cathode or anode and backplane depends quite strongly on geometry. Taking the same data, we find a change of 10 to 40 pF/m for the anode to cathode capacitance as a function of cathode width.

5. Summary

We have written a program that allows us to study in detail the electrostatic field in microstrip gas chambers, including the effects of bulk and surface conductivity of the chamber support. This has allowed us to determine, for a given chamber geometry and choice of materials, a set of potentials resulting in a field configuration that minimizes charging of the support. The program also allows us to determine capacitances and currents between electrodes.

To maximize the gain of the chambers, one can reduce the size of the anodes and/or increase the size of the cathodes. The main limitation here is surface flashover. The thickness of the support is of secondary importance, and can in principle be chosen so as to facilitate readout of the secondary coordinate on the backplane.

References

1. A.Oed, Nucl. Instr. and Meth. A263 (1988) 351

2. F.Angelini et al.,Nucl. Instr. and Meth. A283 (1989) 755

3. H.Hartjes and F.Udo, Proc. ECFA Study Week on Instrum. Techn. for High-Luminosity Hadron Colliders, Barcelona (1989). CERN 89-10 p 455

4. F.Angelini et al.,Proc. ECFA Study Week on Instrum. Techn. for High-Luminosity Hadron Colliders, Barcelona (1989). CERN 89-10 p 465

5. F.Angelini et al.,Proc. IEEE Symposium on Nuclear Science, San Francisco(1990), IEEE Trans. Nucl. Sci. 37, 1990

6. F.Angelini et al., Nucl. Phys. B23A (1991) 254

7. R.Bouclier, J.J.Florent, J.Gaudaen, F.Sauli and L.Shekhtman, Proc. 5th Pisa Meeting on Advanced Detectors,CERN – PPE/91 – 108

8. R.Bouclier et al. Proc. Sixth Int. Wire Chamber Conf., Vienna, 1992

9. A.Brandt, Math. Comp. Vol. 31, 138, pp. 333 – 390

10. E.Durand, *Electrostatique, Tomes I – III* Masson et Cie, Paris (1966)

Figure Captions

Fig. 1.a Field lines for a microstrip chamber with the following geometry: anode width 16 μm, cathode width 160 μm, pitch 384 μm, support thickness 96 μm and drift space 4 mm. Potentials are 650V on the anode, −50V on the backplane, −620V on the drift electrode and 0V on the cathode. The support is assumed to be a perfect insulator with relative dielectric strength $\varepsilon = 3$.

Fig. 1.b Field lines calculated for the same geometry and potentials as Fig.1.a, but with a conducting support.

Fig. 1.c Charge density on the support between anode and cathode for the field configuration shown in Fig.1.b.

Fig. 2 Schematic diagram showing the field lines and quantities used to determine the mapping of the drift electrode on the anode and the optimal field geometry.

Fig. 3 Fraction of anode intercepted by field lines originating on the drift electrode as a function of its voltage. This gives an indication about the fraction of positive ions drifting back towards the drift electrode.

Fig. 4 Field lines calculated for optimized potentials: the geometry and characteristics of the support are the same as in Fig.1 a) and b). The anode, cathode and drift voltages are

also identical to those in Fig.1 a) and b) but the backplane voltage is increased to 153V.

Fig. 5 Experimentally measured gain vs rate for three sets of potentials. Curve 1 corresponds to the optimal field geometry as calculated by MSFIELD

Fig. 6.a Gain vs anode width at fixed anode potential. The anode to anode pitch is fixed at 384 μm, the cathode width is 160 μm and the support thickness is 96 μm.

Fig. 6.b Gain vs cathode width at fixed anode potential. The anode width is 32 μm. All other conditions as in a)

Fig. 6.c Gain vs support thickness at fixed anode potential. The anode width is 32 μm, the cathode width is 160 μm.

Fig. 7 Field lines for a chamber having a support with a 4 μm thick conductive layer, having a resistivity of $10^{11}\Omega$cm, on top of a substrate with resistivity $10^{14}\Omega$cm. The geometry and voltages are the same as those of Fig. 4.

Fig. 8 Electric field strength parallel to the surface between anode and cathode for a chamber with uniform support (solid line) and for a chamber having a 4 μm thick conductive layer on top of the support (dashed line). The dotted lines indicate the edges of the anode and cathode. The anode voltages were adjusted to give identical gas gain in both cases.

Fig. 9.a Anode capacitances vs anode width. Anode to anode pitch is fixed at 384 μm, cathode width is 160 μm and support thickness is 96 μm. The relative dielectric strength of the support is 11.

Fig. 9.b Cathode capacitances vs cathode width. Anode width is fixed at 32 μm, everything else as in a)

Fig. 9.c Anode and cathode capacitances vs support thickness. Anode width is 32 μm, cathode width 160 μm, everything else as in a)

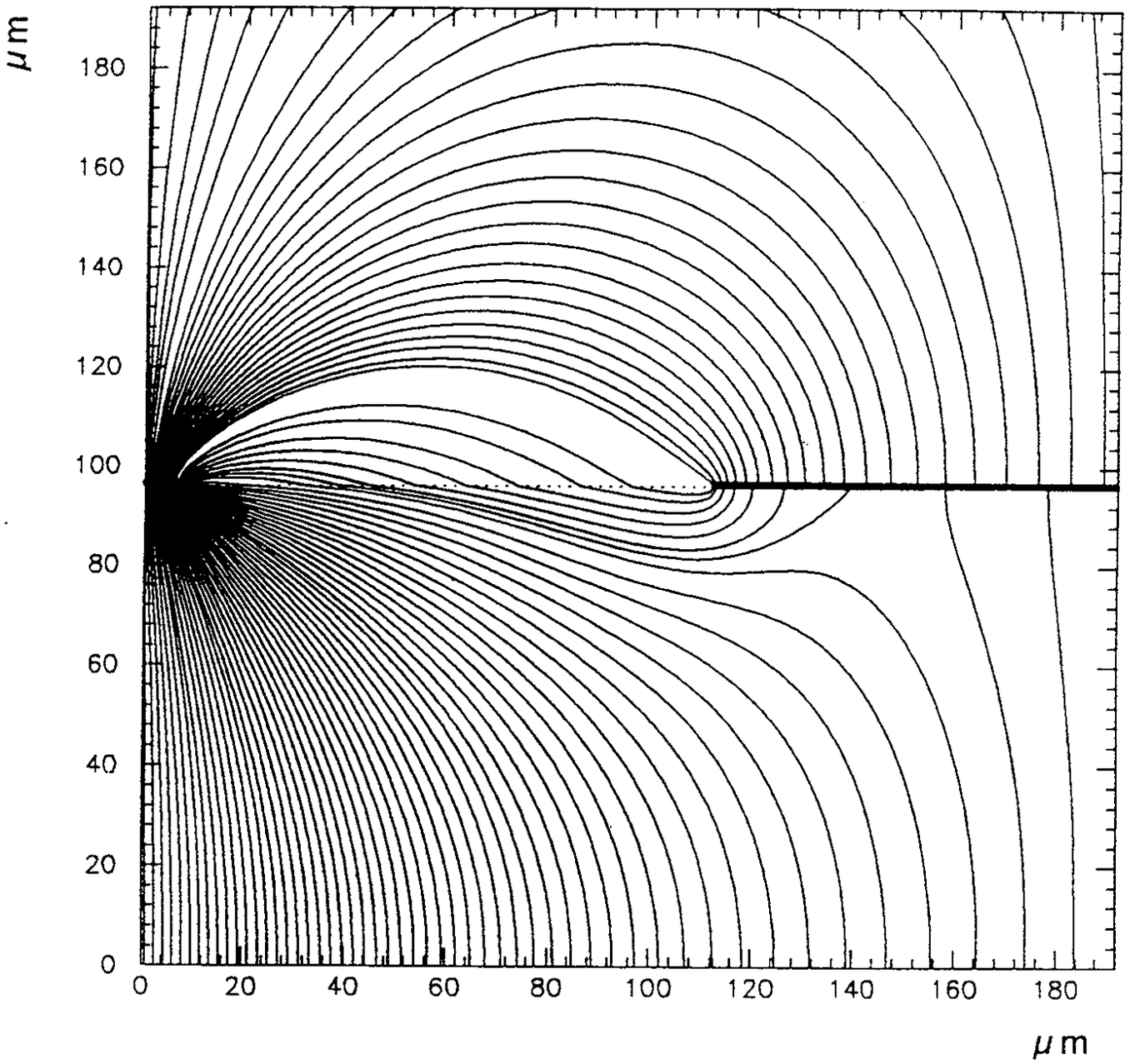
μm
180
160
140
120
100
80
60
40
20
0
0
20
40
60
80
100
120
140
160
180
μm

Fig. 1.a

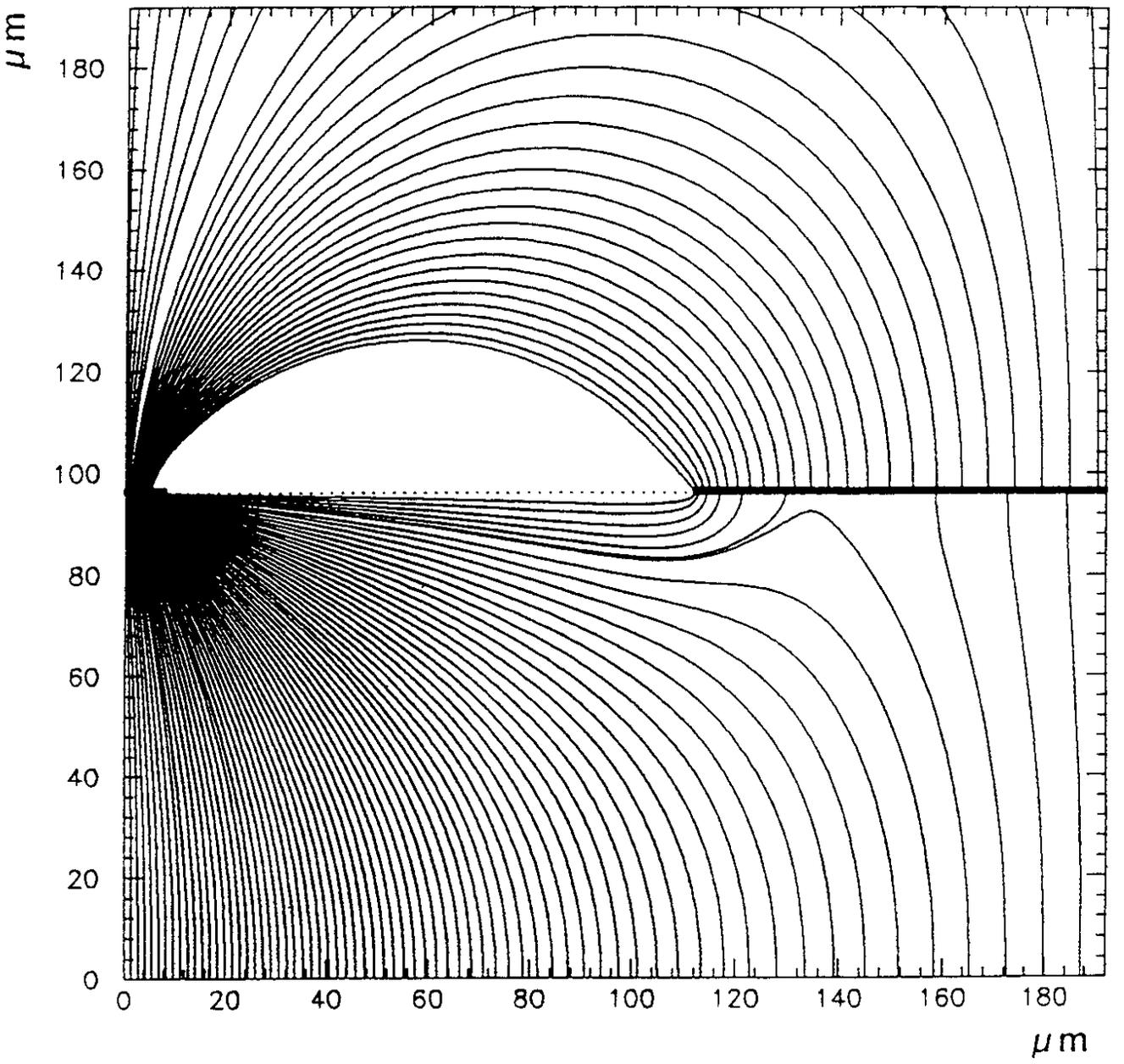
μm
180
160
140
120
100
80
60
40
20
0
0
20
40
60
80
100
120
140
160
180
μm

Fig. 1.b

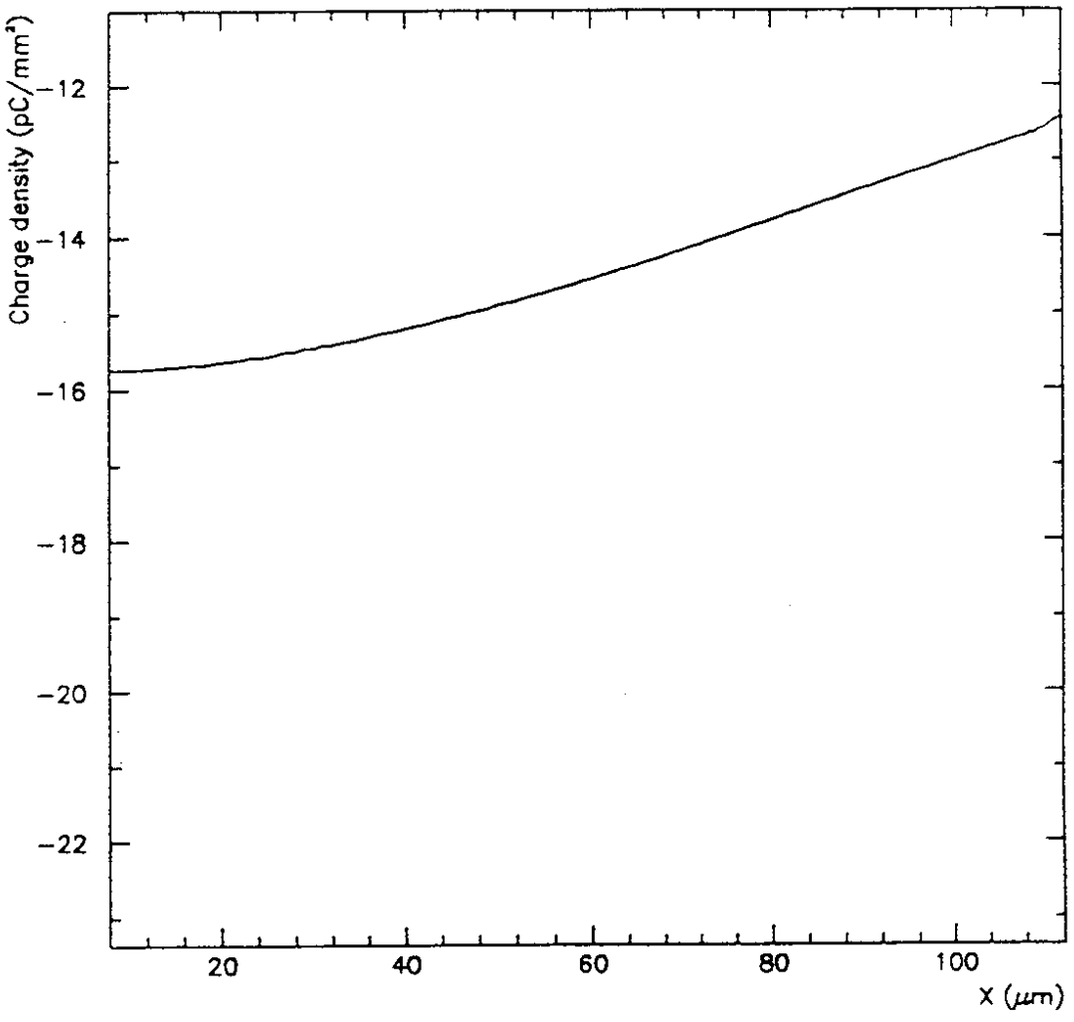

Fig. 1.c

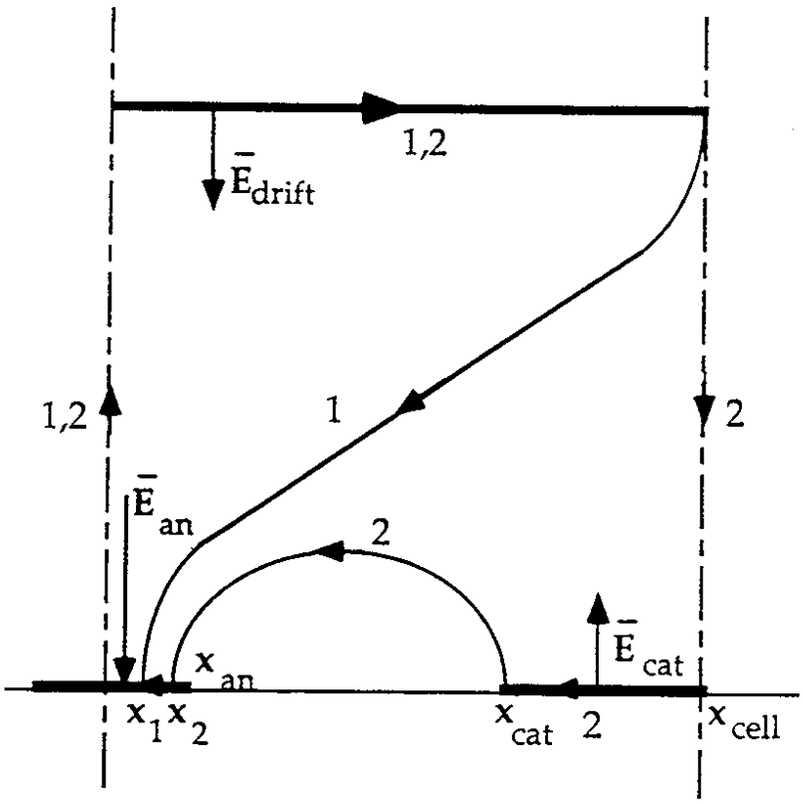

Fig. 2

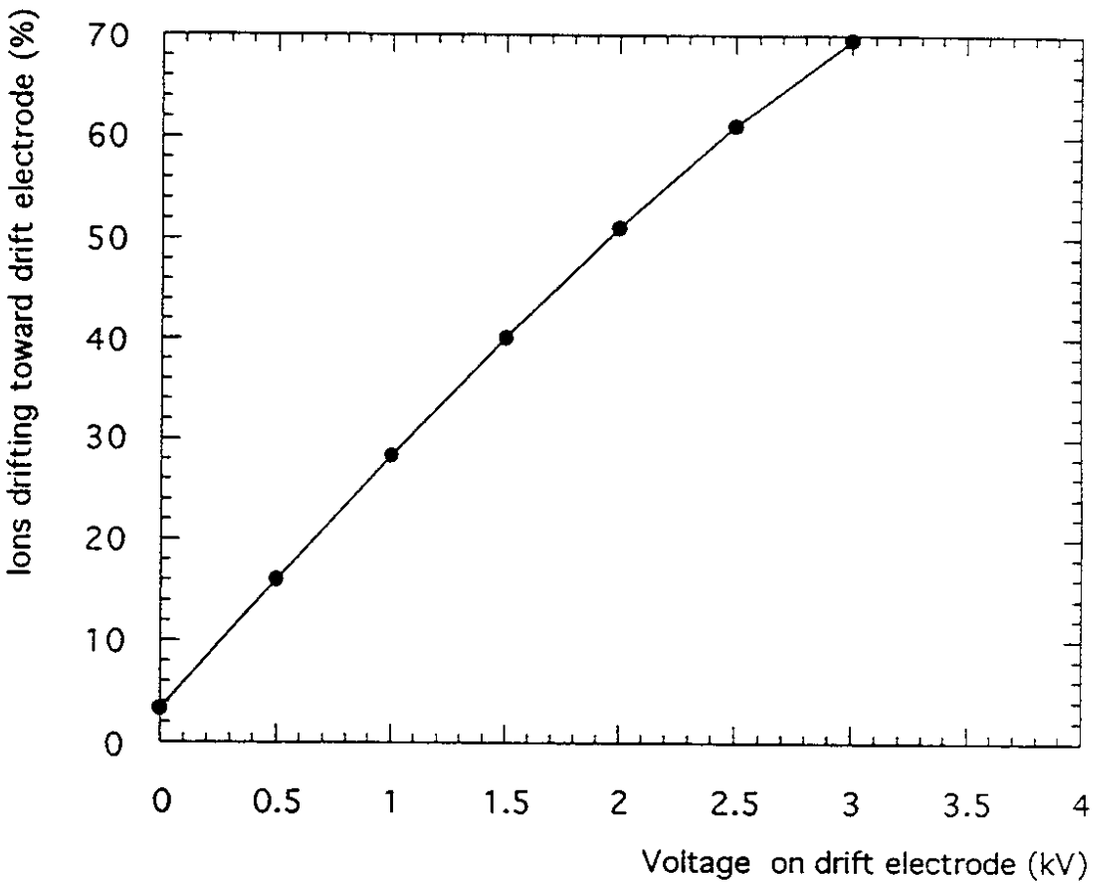
Ions drifting toward drift electrode (%)
70
60
50
40
30
20
10
0
0
0.5
1
1.5
2
2.5
3
3.5
4
Voltage on drift electrode (kV)

Fig. 3

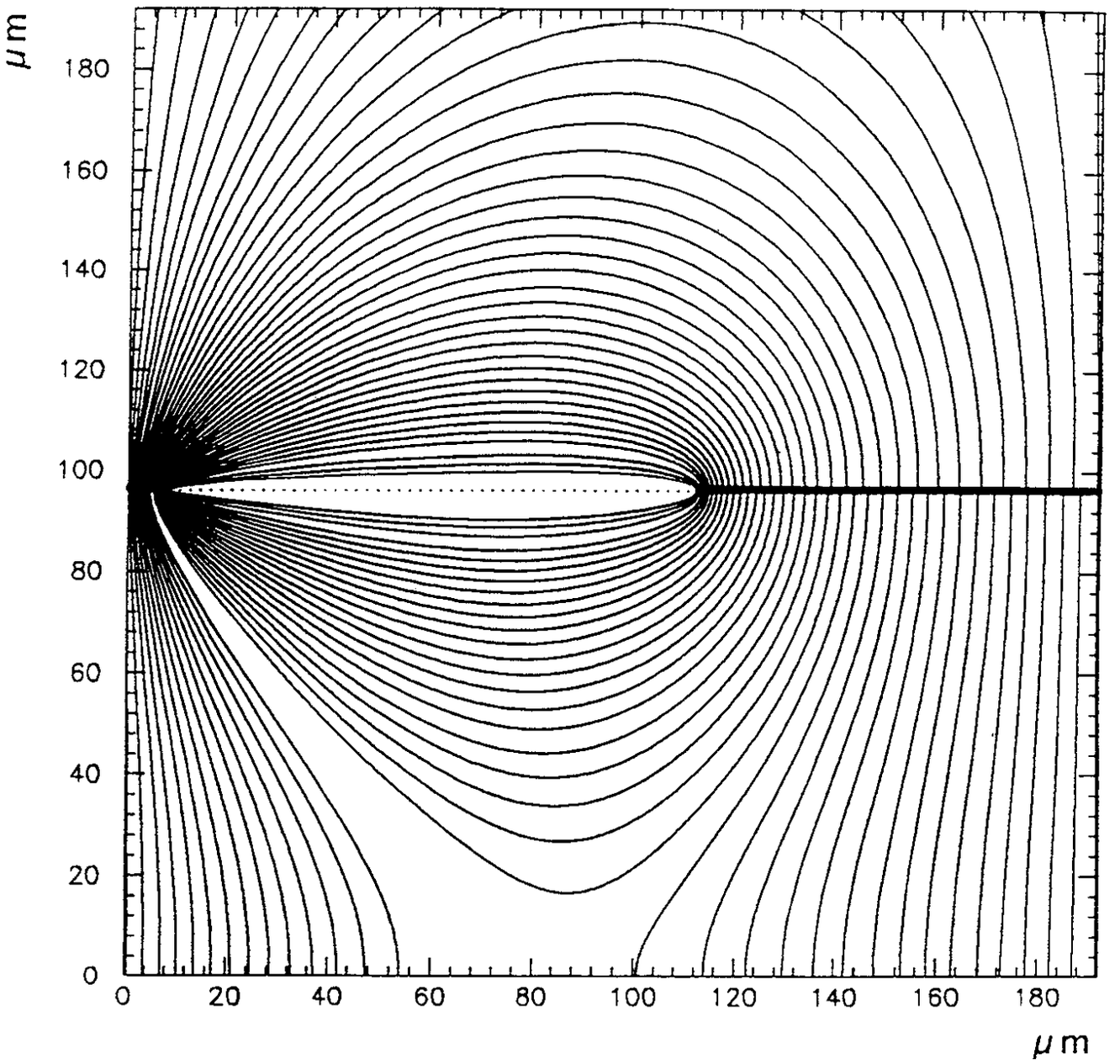
μm
180
160
140
120
100
80
60
40
20
0
0
20
40
60
80
100
120
140
160
180
μm

Fig. 4

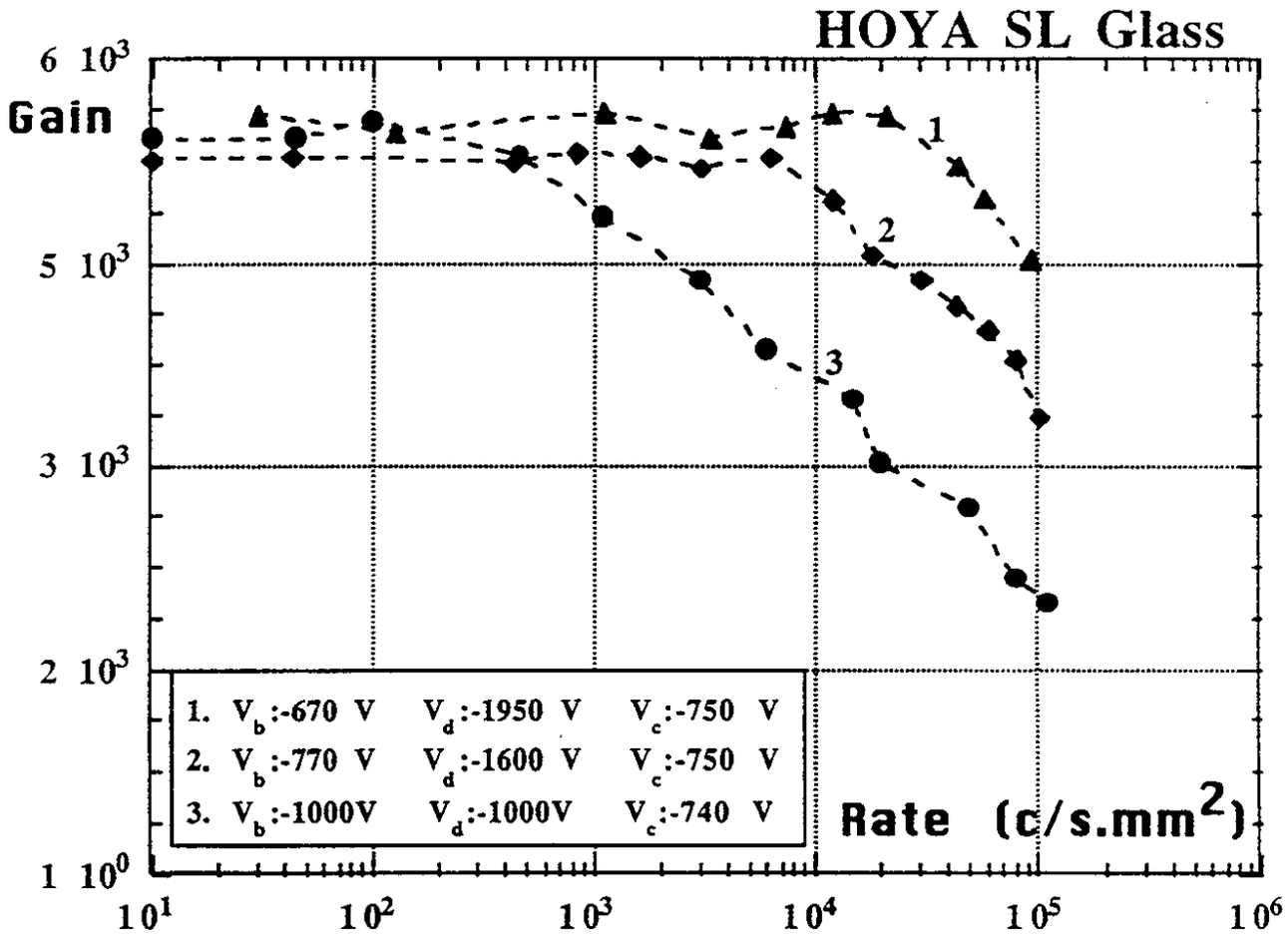
HOYA SL Glass
Gain
6 10^3
5 10^3
3 10^3
2 10^3
1 10^0
10^1
10^2
10^3
10^4
10^5
10^6
1
2
3
1. V_b:-670 V V_d:-1950 V V_c:-750 V
2. V_b:-770 V V_d:-1600 V V_c:-750 V
3. V_b:-1000V V_d:-1000V V_c:-740 V
Rate (c/s.mm^2)

Fig. 5

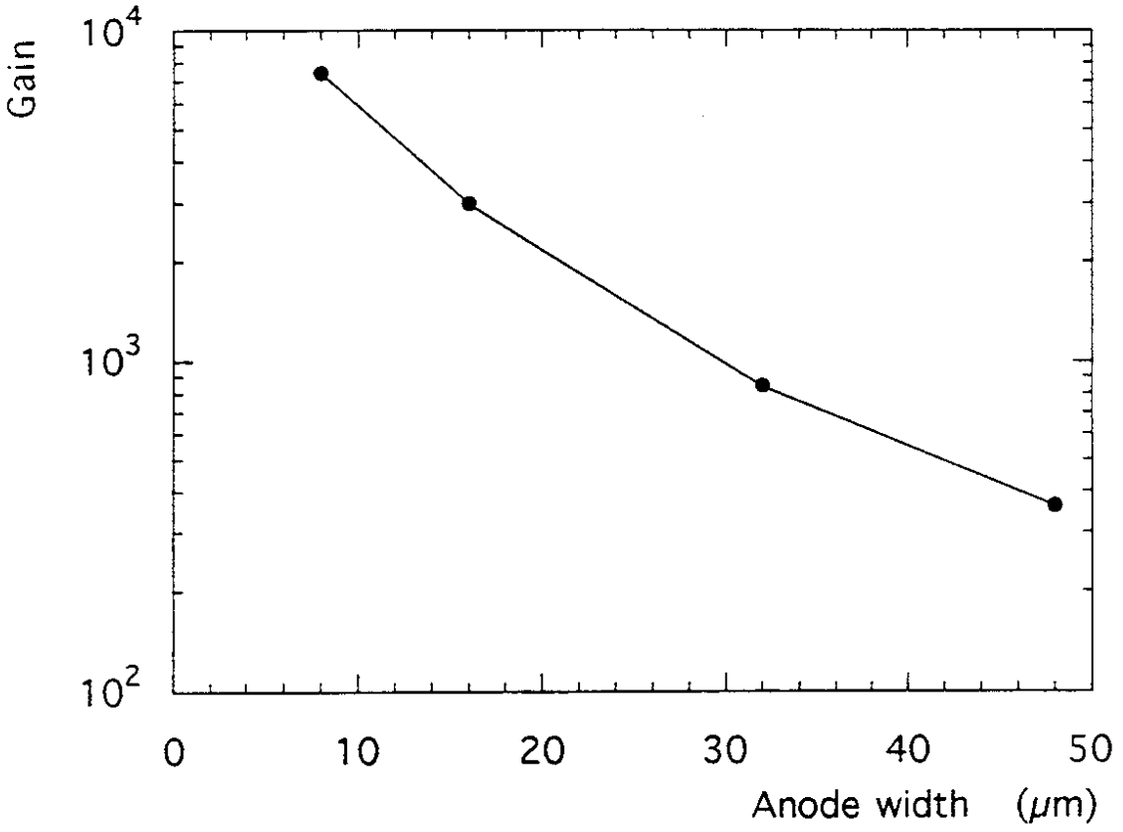

Fig. 6a

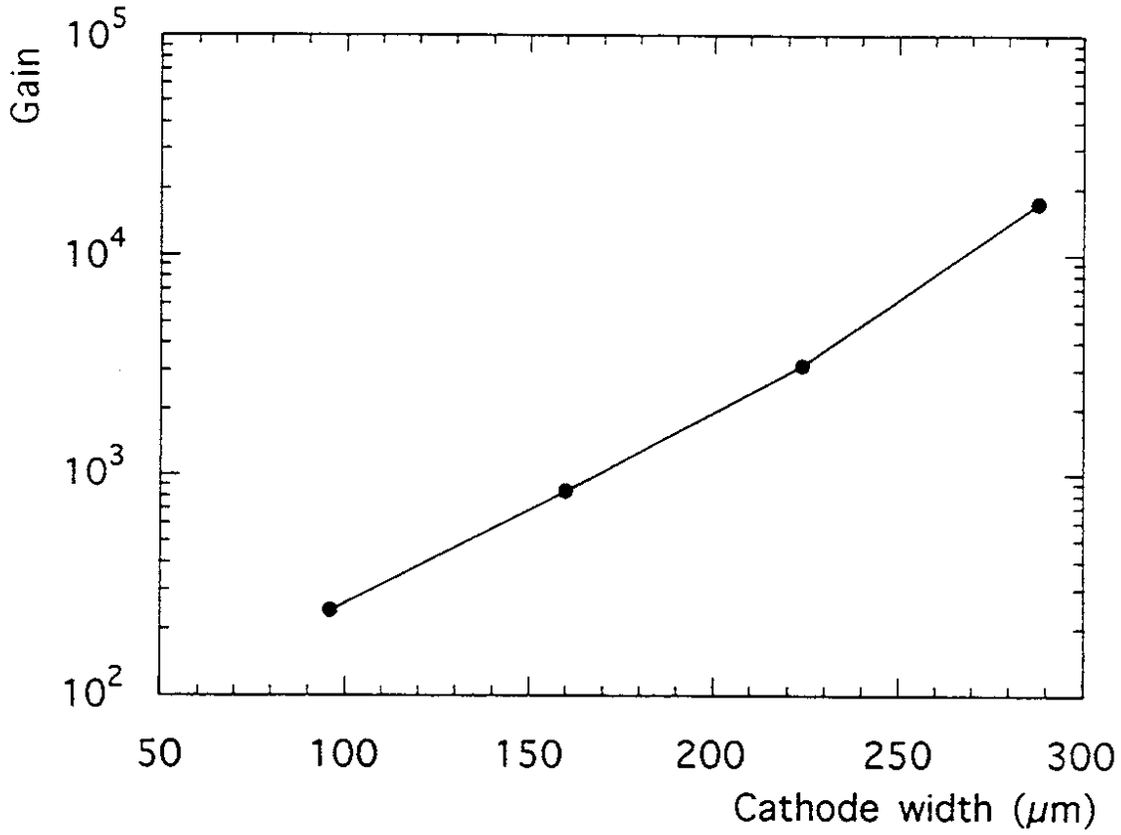

Fig. 6b

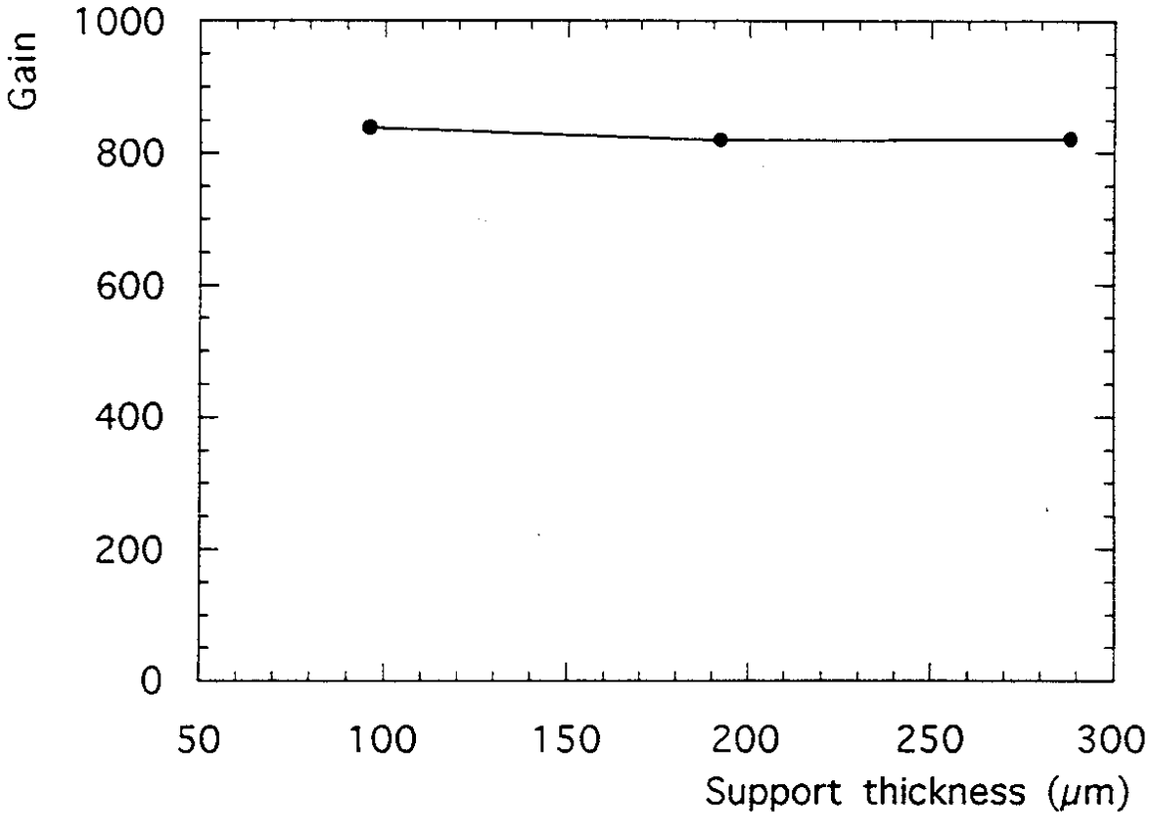
Gain
1000
800
600
400
200
0
50
100
150
200
250
300
Support thickness (μm)

Fig. 6c

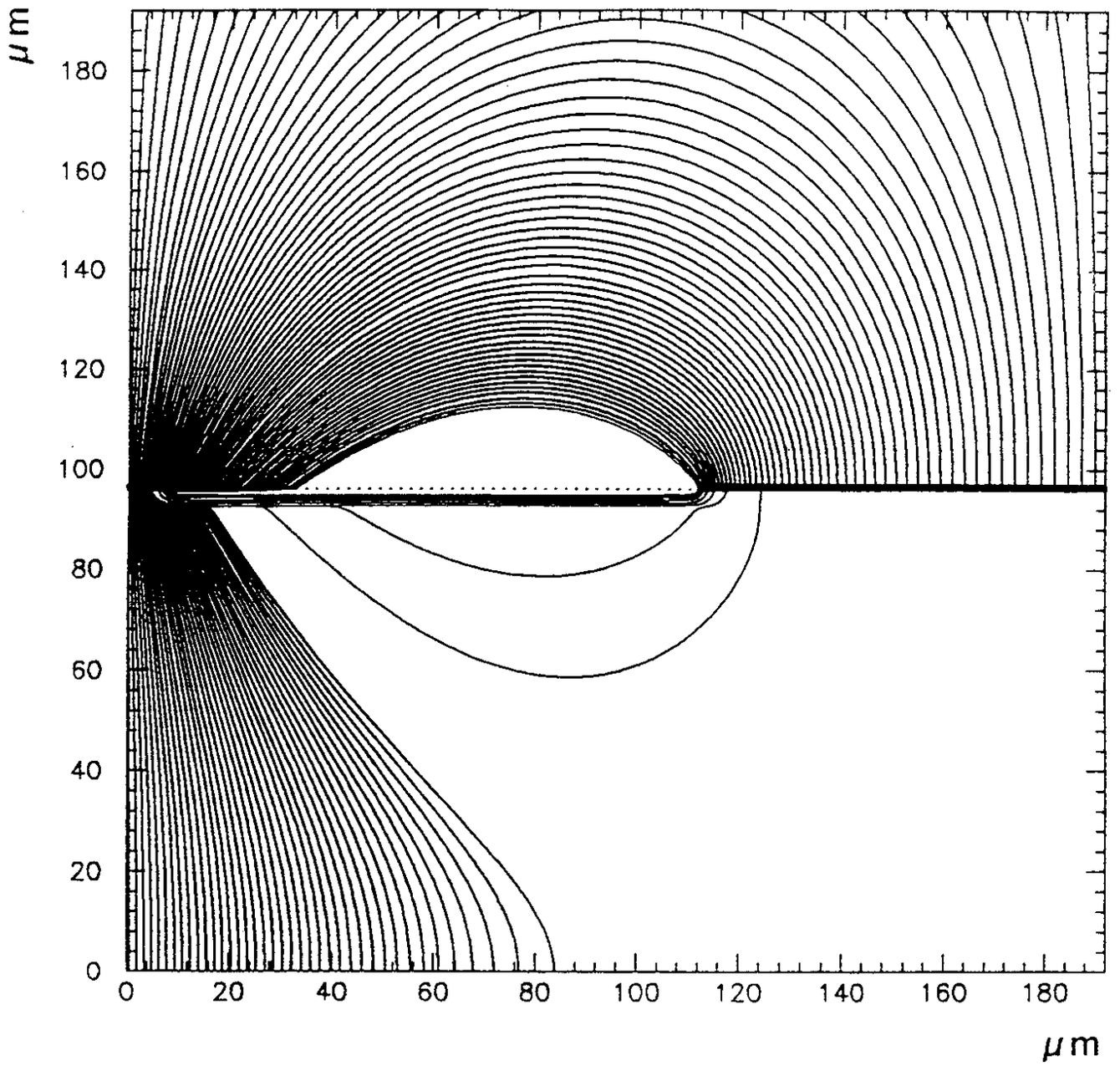
μm
180
160
140
120
100
80
60
40
20
0
0
20
40
60
80
100
120
140
160
180
μm

Fig. 7

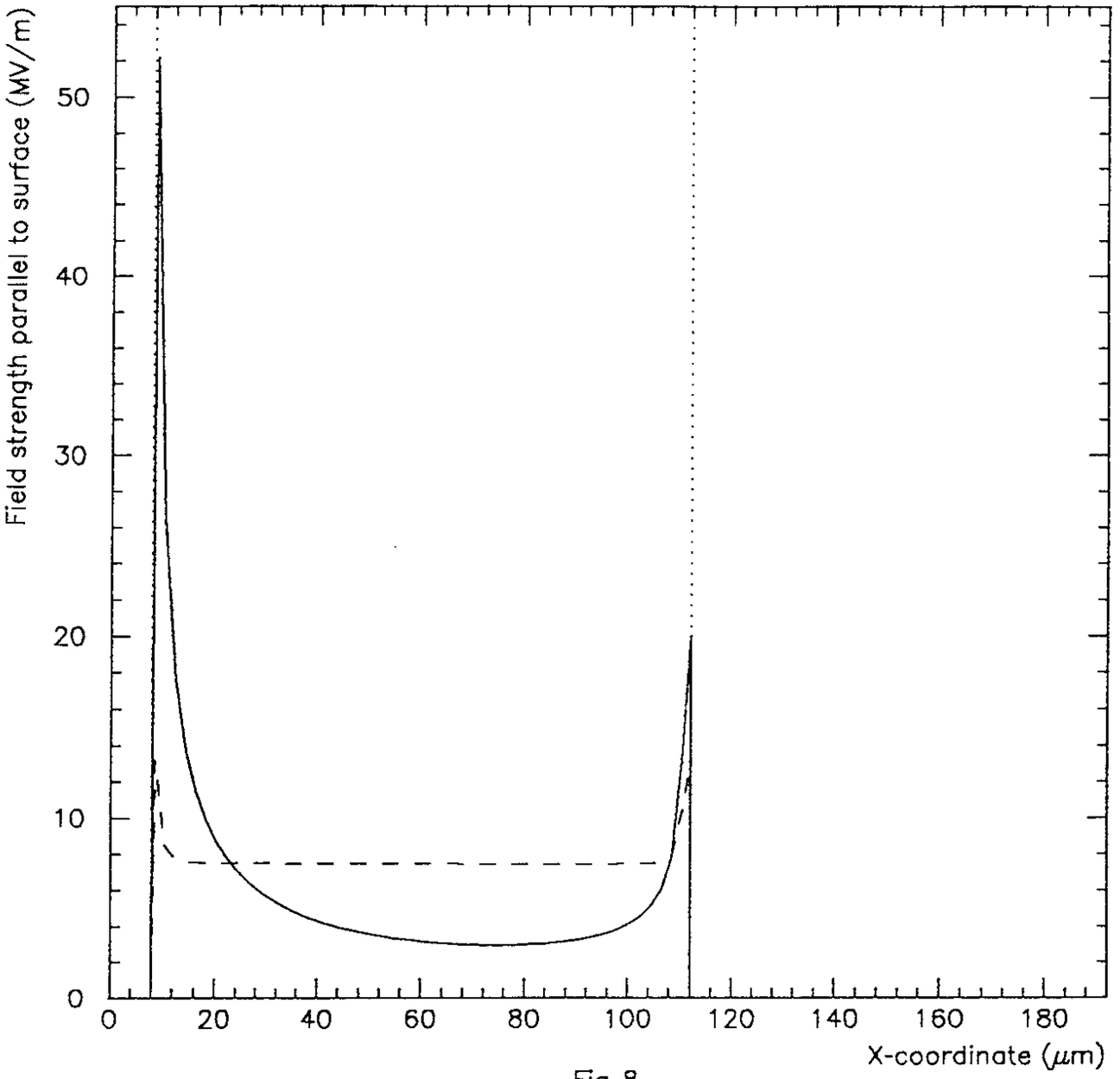
Field strength parallel to surface (MV/m)
50
40
30
20
10
0
0
20
40
60
80
100
120
140
160
180
X-coordinate (μm)

Fig. 8

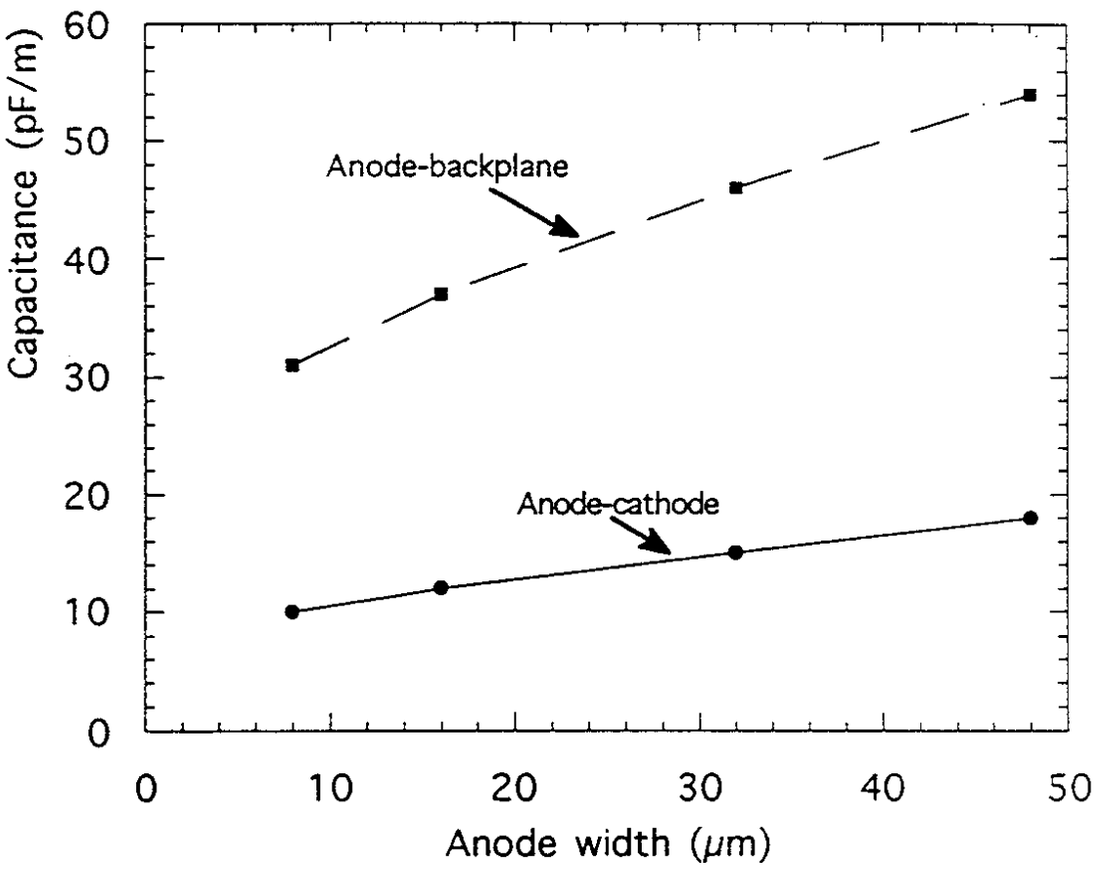
Capacitance (pF/m)
60
50
40
30
20
10
0
Anode-backplane
Anode-cathode
0
10
20
30
40
50
Anode width (μm)

Fig. 9a

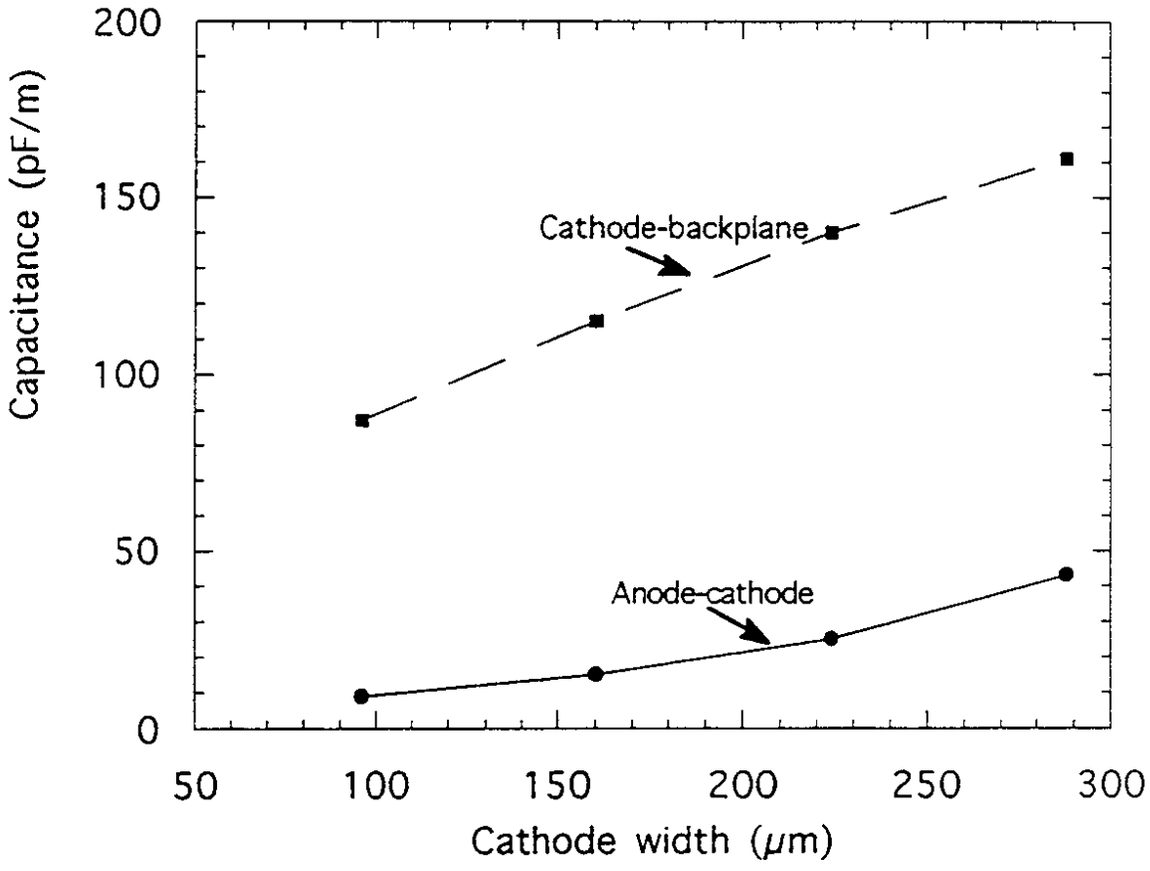
200
150
100
50
0
Capacitance (pF/m)
Cathode-backplane
Anode-cathode
50
100
150
200
250
300
Cathode width (μm)

Fig. 9b

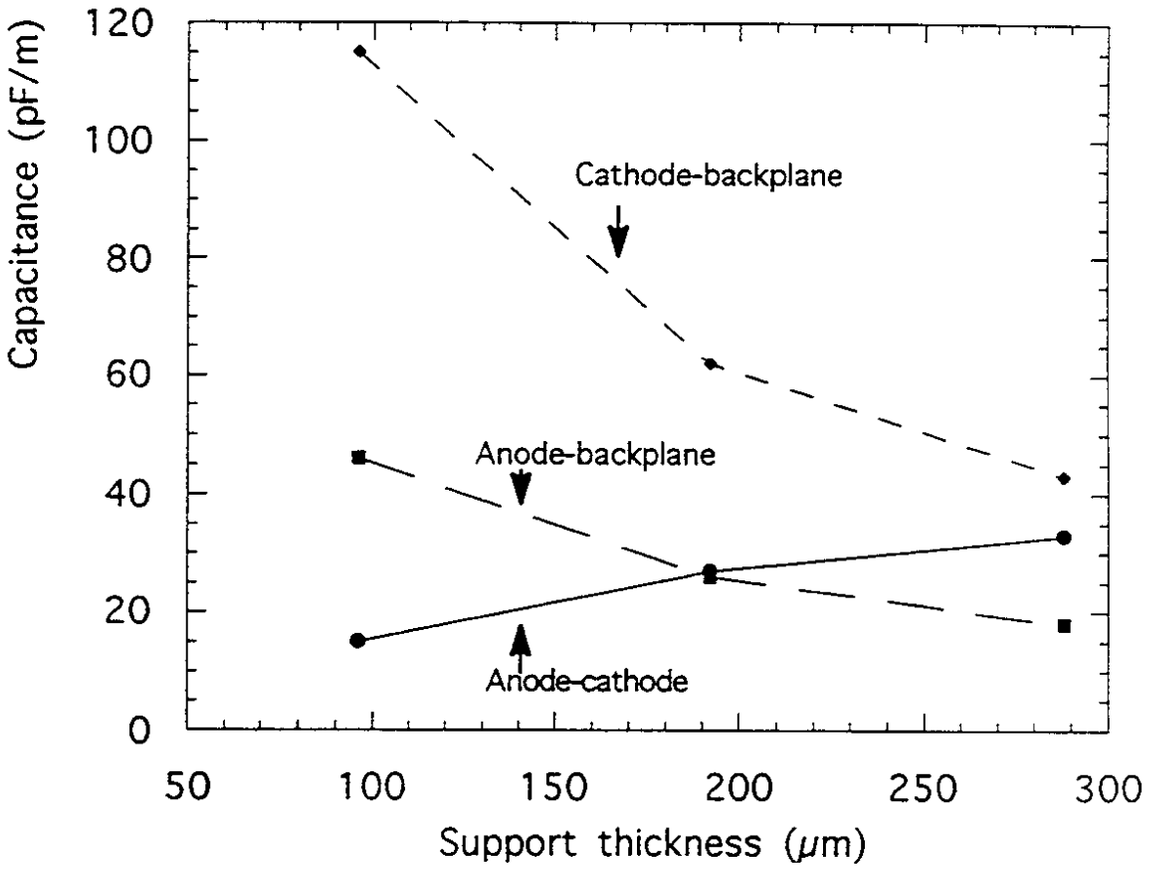
Capacitance (pF/m)
120
100
80
60
40
20
0
50
100
150
200
250
300
Support thickness (μm)
Cathode-backplane
Anode-backplane
Anode-cathode

Fig. 9c